Quantum thermodynamics of periodically driven polaritonic systems

Maicol A. Ochoa*

Department of Chemistry and Biochemistry, University of Maryland, College Park, Maryland, USA

(Received 8 June 2022; revised 10 November 2022; accepted 16 November 2022; published 8 December 2022)

We investigate the energy distribution and quantum thermodynamics in periodically-driven polaritonic systems in the stationary state at room temperature. Specifically, we consider an exciton strongly coupled to a harmonic oscillator and quantify the energy reorganization between these two systems and their interaction as a function of coupling strength, driving force, and detuning. After deriving the quantum master equation for the polariton density matrix with weak environment interactions, we obtain the dissipative time propagator and the long-time evolution of an equilibrium initial state. This approach provides direct access to the stationary state and overcomes the difficulties found in the numerical evolution of weakly damped quantum systems near resonance, also providing maps on the polariton lineshape. Then, we compute the thermodynamic performance during harmonic modulation and demonstrate that maximum efficiency occurs at resonance. We also provide an expression for the irreversible heat rate and numerically demonstrate that this agrees with the thermodynamic laws.

DOI: 10.1103/PhysRevE.106.064113

I. INTRODUCTION

Hybrid polaritonic states, resulting from the interaction between excitons and photons, manifests on systems such as molecules in cavities [1,2], plexcitons [3–5], optically-stimulated semiconductors [6–10], and nanomechanical devices [11–13]. Excitonic polaritons display distinct properties that frequently depart from those of their components, providing an ideal platform for the investigation of strong coupling emergence, hybrid-state formation, their quantum control, and potential quantum technologies [14]. For foundational and practical reasons, it is interesting to study polaritons as nanoscale devices and, in particular, address their stability and performance under modulation due to external fields and forces.

Quantum thermodynamics [15–19] aims to extend thermodynamic concepts, such as work [20], heat [15,21,22], entropy [16,23], and efficiency [24] to nonequilibrium systems with a few degrees of freedom, evolving in regimes where quantum fluctuations cannot be ignored. Studies in this field have concentrated on dissipative fermionic [16,25–27] and bosonic [28] systems under slow [29–31] or periodic modulation, and different techniques to describe periodically driven nanoscale systems are continuously emerging based on reduced quantum master equations [32–34] and Floquet theory [35–37]. Of particular interests are nanoscale systems and quantum materials resulting from light-matter interactions [34,38,39]. Frequently, the dynamic and thermodynamic representation of these systems appear to be contradictory, especially when the interaction term, responsible for appearance of hybrid states, is of the same order of magnitude than the system energy [25,40], such as in the case of strongly coupled polaritons. Recent studies in the polariton dynamics [41–44] attempt to account for dissipation in open or lossy systems.

In this paper, we report on the quantum thermodynamics of periodically driven dissipative polaritons, characterizing the stationary energy and population distribution. Our model describes weakly damped polaritons coupled to heat and work reservoirs, providing direct access to the stationary state and the absorption lineshape in terms of damping parameters, exciton-phonon coupling, and detuning from the driving field frequency. Remarkably, our thermodynamic analysis reveals that the energy dissipated to the environment in the stationary state in the form of heat is related to the polariton von Neumann entropy.

II. POLARITON DYNAMICS

We consider a composite $\hat{H}_{\rm S}$ consisting of a two-level electronic system and a phonon, interacting with the environment $\hat{H}_{\rm B}$ and with interaction energy $\hat{H}_{\rm I} = \hat{H}_{\rm IX} + \hat{H}_{\rm IP}$ given by ($\hbar = 1$)

$$\hat{H} = \hat{H}_{\rm S} + \hat{H}_{\rm I} + \hat{H}_{\rm B}, \tag{1}$$

$$\hat{H}_{\rm S} = \sum_{i=1}^{2} \varepsilon_i \hat{d}_i^\dagger \hat{d}_i + \omega \hat{a}^\dagger \hat{a} + V \hat{d}_2^\dagger \hat{d}_1 \hat{a} + V^* \hat{a}^\dagger \hat{d}_1^\dagger \hat{d}_2, \tag{2}$$

$$\hat{H}_{\rm IX} = \sum_k W_k^X \hat{c}_k^\dagger \hat{d}_1^\dagger \hat{d}_2 + W_k^{X*} \hat{d}_2^\dagger \hat{d}_1 c_k, \tag{3}$$

$$\hat{H}_{\rm IP} = \sum_k W_k^P \hat{b}_k^\dagger \hat{a} + \text{ h.c}\,. \tag{4}$$

The Hamiltonian $\hat{H}$ in Eq. (1) is reminiscent of the Jaynes-Cummings model and incorporates explicitly energy damping to the environment. In Eq. (2), ε_i is the ith level energy, ω is the characteristic frequency for the phonon, $\hat{d}_i^\dagger$ ($\hat{d}_i$) is the creation (annihilation) operator for an electron in the ith level,

*maicol@umd.edu

$\hat{a}^\dagger$ ($\hat{a}$) creates (annihilates) a phonon, and V is the coupling term between the phonon and the two-level system. The electronic and phononic components of the system interact with the corresponding bosonic baths, namely, $\hat{H}_X = \sum_k \varepsilon_k \hat{c}_k^\dagger \hat{c}_k$ and $\hat{H}_P = \sum_k \omega_k \hat{b}_k^\dagger \hat{b}_k$, with coupling terms W_k^X and W_k^P as in Eqs. (3) and (4). These represent the heat reservoirs, which account for dissipative interactions with the environment. In the exciton case, these occur via radiative decay, energy damping via vibrational relaxation, or other nonradiative mechanisms. In the phonon case, dissipation occurs via couplings to different modes in the system or, in the case of a Fabry-Perot cavity, energy losses due to mirror leakage or absorption.

As a consequence of the electron-phonon coupling, hybrid states $|\alpha\rangle$ are formed. These hybrid states diagonalize $\hat{H}_S$, with corresponding eigenenergies λ_α and, in general, differ from the product states $|i, m\rangle$ characterized by the electronic quantum number i and phonon mode m. To bring the polariton in a nonequilibrium condition, we consider the following generic periodic time-dependent variation, with frequency ω' and interaction strength A

$$\hat{H}_d(t) = 2A\cos(\omega' t)\sum_m |1, m\rangle\langle m, 2| + |2, m\rangle\langle m, 1|, \quad (5)$$

and obtain a dynamical description of the driven polariton by solving the Liouville-von Neumann equation for the full density matrix. The Hamiltonian $\hat{H}_d(t)$ describes the exciton interaction with an unspecified reversible work reservoir [45]. Physically, the work reservoir can be an incident electromagnetic field coupled to the exciton via dipole-field interactions. We solve the Liouville equation in the interaction picture with interacting Hamiltonian $\hat{H}_d(t) + \hat{H}_I$, invoking the Born-Markov approximation [46] (see Appendix A for details). In this form, our solution is valid to second order in W^X, W^P, and A; holds for arbitrary values in the coupling term V. The resulting Markovian equation for the reduced density matrix $\rho(t)$ is

$$\frac{d}{dt}\vec{\rho}(t) = -(\mathcal{D} + \mathcal{L}_X + \mathcal{L}_P + \mathcal{L}_d(t))\vec{\rho}(t), \quad (6)$$

where we write the reduced density matrix as a vector $\vec{\rho}(t)$ with elements $\rho_\alpha^\beta(t) = \langle\alpha|\rho(t)|\beta\rangle$. In Eq. (6), the operator $\mathcal{D}$ is diagonal with matrix element $\mathcal{D}_{\alpha_2\beta_2}^{\alpha_1\beta_1} = -i(\lambda_{\alpha_1} - \lambda_{\beta_1})\delta_{\alpha_1}^{\alpha_2}\delta_{\beta_1}^{\beta_2}$ and corresponds to the free evolution of the polariton in the absence of any relaxation mechanism; $\mathcal{L}_X$ and $\mathcal{L}_P$ are operators that result from the independent exciton and phonon relaxation and are correspondingly proportional to the damping rates $\Gamma_\square = 2\pi\sum_k |W_k^\square|^2\delta(\omega_k - \omega)$ with $\square = X, P$. The time-dependent operator $\mathcal{L}_d(t)$ introduces the effects of the driving field in the polariton state, in a form that is proportional to A^2 and that depends on the frequency of the incident field ω'. Notably, $\mathcal{L}_d(t)$ is periodic with period $\tau = 2\pi/\omega'$ (see Appendix A for details).

Formally, in the representation chosen in Eq. (6), the reduced density matrix has an infinite (countable) number of matrix elements. Due to the relaxation induced by the couplings to the environment, the contributions to the dynamics from higher energy states can be disregarded and a finite matrix representation of the operators in Eq. (6), in terms of the hybrid states formed by the lowest m_o phonon modes, results in a faithful approximation to the dynamics. Within this finite representation, the $\mathcal{L}$ operators are $(2m_o)^2$-square matrices, and the time-dependent reduced density matrix obtained from the initial equilibrum condition $\vec{\rho}(0)$ is

$$\vec{\rho}(t) = \exp\left[-(\mathcal{D} + \mathcal{L}_X + \mathcal{L}_P)t - \int_0^t \mathcal{L}_d(t')dt'\right]\vec{\rho}(0). \quad (7)$$

Utilizing the $\mathcal{L}_d$ periodicity we find that for $t = N\tau + \Delta t$, $\Delta t < \tau$

$$\int_0^t \mathcal{L}_d(t')dt' = \pi A^2\left(\frac{t}{2} - i\frac{e^{2i\omega'\Delta t}}{4\omega'}\right)\mathcal{N}_+ + \pi A^2\left(\frac{t}{2} + i\frac{e^{-2i\omega'\Delta t}}{4\omega'}\right)\mathcal{N}_-, \quad (8)$$

where $\mathcal{N}_\pm$ are time-independent transition matrices describing the allowed system state conversions due to the external modulation. We note that the operator in Eq. (8) is a time-local matrix and, as a result, the evolution operator in Eq. (7) is well-defined without a time-ordering operator.

Equations (7) and (8) provide a simple description of a weakly damped periodically-modulated polariton in the strong coupling regime, as it holds for arbitrary values for the electron-phonon coupling strength V. Moreover, Eq. (7) constitutes a numerically stable model for the dynamics of the driven system, naturally incorporating the effects of the system-bath couplings (system-bath coherences) within the Markovian regime, and allowing direct investigation of the polariton long-time evolution. In contrast, the numerical propagation of Eq. (6) demands the initial evolution of the free system to introduce system-bath correlations and may not be stable near the resonance condition ($\omega = \omega'$), as in this case Eq. (6) becomes a stiff differential equation. In this form, Eqs. (7) and (8) overcome the difficulties found in the study of lossy cavities [47] near resonance [48], in the long-time evolution regime, and for an arbitrary driving frequency ω'. Significantly, Eqs. (7) and (8) are not limited to slow driving rates and do not require time-coarse graining [32] to describe the system in the long-time evolution limit.

III. POLARITON THERMODYNAMICS

Starting from Eq. (6), we define elementwise the time-dependent operators L_X, L_P, and L_d corresponding to the different partial time derivatives of the polariton density matrix

$$L_{\square\,\alpha_1}^{\beta_1} = \sum_{\alpha_2\beta_2} \mathcal{L}_{\square\,\alpha_2\beta_2}^{\alpha_1\beta_1}\rho_{\alpha_2}^{\beta_2}(t) \quad (\square = X, P, d), \quad (9)$$

and identify two reversible heat rates due to the polariton-heat reservoir interaction

$$\dot{Q}_X(t) = -\mathrm{Tr}[L_X(t)\hat{H}_S], \quad (10)$$

$$\dot{Q}_P(t) = -\mathrm{Tr}[L_P(t)\hat{H}_S]. \quad (11)$$

Similar considerations were used in, e.g., Ref. [34] to define heat rates in dissipative driven TLS. Since we chose an

interaction representation that includes the driving field $\hat{H}_d(t)$ in the interaction term, the power or work rate on the polariton due to this external modulation is given by

$$\dot{W}(t) = -\mathrm{Tr}[L_d(t)\hat{H}_S]. \tag{12}$$

The polariton's von Neumann entropy

$$S(t) = -\mathrm{Tr}[\rho(t)\ln\rho(t)] \tag{13}$$

significantly differs from the sum of the exciton and phonon residual entropies in the strong-coupling regime. However, the total entropy change rate is the linear combination of three different rates resulting from interactions with the environment

$$\dot{S}(t) = \dot{S}_X(t) + \dot{S}_P(t) + \dot{S}_d(t), \tag{14}$$

$$\dot{S}_\square = \mathrm{Tr}[L_\square(t)\ln\rho(t)] \quad (\square = X, P, d). \tag{15}$$

Ideally, to consider the information entropy in Eq. (13), or any other, as the polariton nonequilibrium entropy function, its connection with the dissipated energy in the form of heat should closely follow the Clausius theorem. Thus, in terms of the reversible heat and entropy rates, we define the effective polariton temperature β_{eff} as the proportionality factor between the total reversible heat rate and the sum of the associated entropy rates

$$\beta_{\mathrm{eff}}(\dot{Q}_X(t) + \dot{Q}_P(t)) = \dot{S}_X(t) + \dot{S}_P(t). \tag{16}$$

In this form, β_{eff} has units of inverse energy and may fluctuate as the driving field. We assess the significance of β_{eff} by analyzing energy conservation. The first law imposes that the internal energy variation for the universe, $\dot{U}_{\mathrm{univ}}$, must always vanish. Consequently, $\dot{U}_S + \dot{U}_X + \dot{U}_P + \dot{U}_W = 0$, where U_W is the work source internal energy. Since the thermal reservoirs are assumed to be reversible, then $\dot{U}_X = -\dot{Q}_x$, $\dot{U}_P = -\dot{Q}_p$. We identify an additional energy rate, $\beta_{\mathrm{eff}}^{-1}\dot{S}_d$, between the polariton and the work source. Assuming that the work source volume is fixed, we conclude that $\dot{U}_W = -\beta_{\mathrm{eff}}^{-1}\dot{S}_d$.

Finally, relative to the polariton equilibrium density matrix $\rho_o = e^{-\beta_o\hat{H}_S}/\mathrm{Tr}[e^{-\beta_o\hat{H}_S}]$, where $\beta_o = 1/(k_B T_{\mathrm{env}})$ and T_{env} is the environment temperature, we define the irreversible heat rate by invoking the Spohn theorem [30,31,49]

$$\begin{aligned}\dot{Q}_{\mathrm{irrev}}(t) &= \beta_o^{-1}\mathrm{Tr}[(\mathcal{L}_X(t) + \mathcal{L}_P(t))(\ln\rho_o - \ln\rho(t))] \\ &= \beta_o^{-1}(\dot{S}_X(t) + \dot{S}_p(t)) - (\dot{Q}_x(t) + \dot{Q}_P(t)).\end{aligned} \tag{17}$$

IV. NUMERICAL EXAMPLE

We now consider a driven dissipative polariton with identical driving field, phonon, and exciton frequencies (specifically $\omega' = \omega = \varepsilon_2 = 1$ eV, and $\varepsilon_1 = 0$) with driving parameter $A = 0.1$ eV, initially at the ground state (such that $\rho_\alpha^\beta(0) = \delta_{\alpha,(0,0)}\delta_{\beta,(0,0)}$ in the $|i,m\rangle$ basis). For this system, $\hat{H}_S$ is a block matrix with eigenvalues $\lambda_n^\pm = (n+1)\omega \pm V$ and zero. Figure 1(a) shows the phonon energy $E_{\mathrm{pho}} = \omega\langle\hat{a}^\dagger\hat{a}\rangle$, the exciton energy $E_{\mathrm{TLS}} = \varepsilon_2\langle\hat{d}_2^\dagger\hat{d}_2\rangle$, the interaction energy $E_{\mathrm{int}} = V\langle(\hat{d}_2^\dagger\hat{d}_1\hat{a} + \hat{a}^\dagger\hat{d}_1^\dagger\hat{d}_2)\rangle$, and the total polariton energy $\langle\hat{H}_S\rangle$ as a function of coupling strength V at 300 K and after propagating the system 8.271 ps (2000τ). In Fig. 1 we assume

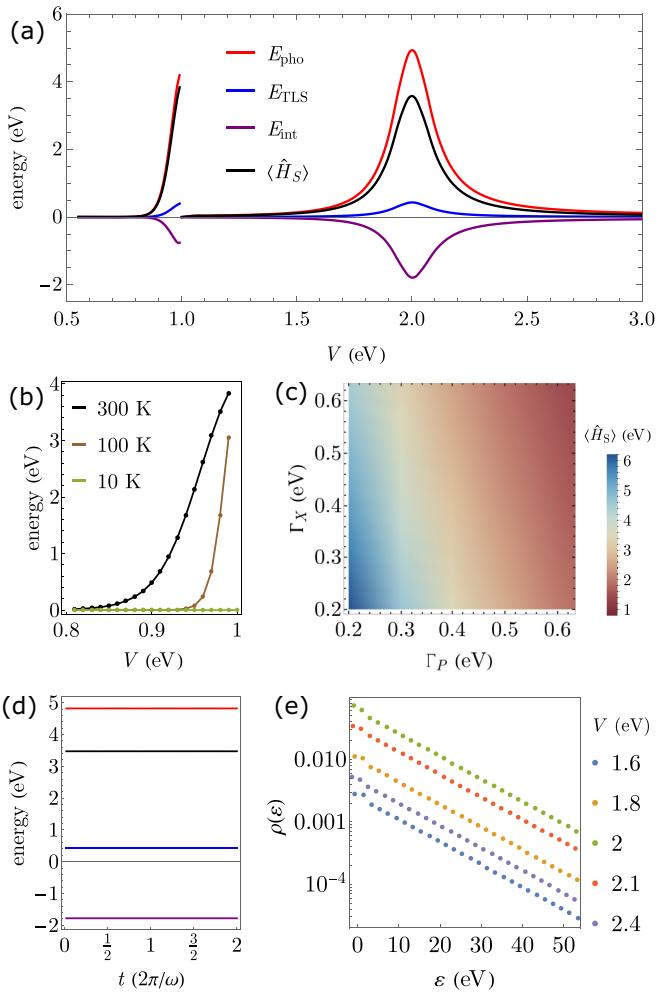

FIG. 1. Polariton energy distribution. (a) Stationary phonon, exciton, interaction, and polariton energies, respectively denoted by E_{pho}, E_{TLS}, E_{int}, and $\langle\hat{H}_S\rangle$), as a function of coupling strength V. (b) $\langle\hat{H}_S\rangle$ near $V = \omega$ calculated at three different bath temperatures: 300 K (black), 100 K (brown), 10 K (green). (c) $\langle\hat{H}_S\rangle$ at resonance ($V = 2\omega$) as function of the damping parameters Γ_X, Γ_P. (d) Phonon, exciton, interaction, and polariton energies as a function of time, and after a propagation period of 8.721 ps. (color code as in panel (a). (e) Diagonal density matrix elements in the product state basis, as a function of energy and for several V. Parameters are $\omega' = \omega = 1.0$ eV, $\Gamma_X = 0.2$ eV, $\Gamma_P = 0.4$ eV, $A = 0.1$ eV, $\varepsilon_1 = 0$ eV, $\varepsilon_2 = 1$ eV, $T = 300$ K, unless otherwise specified.

the wideband limit and set the damping rates to $\Gamma_X = 0.2$ eV and $\Gamma_P = 0.4$ eV and include the lowest 30 phonon modes, which was enough to achieve numerical convergence in the rates (see Appendix B for additional details). As we vary the coupling strength V, we find two significant features in the energy. First, we observe a monotonic increase in the absolute energies starting around $V = 0.85$ eV with a sudden decay at 1 eV; and second, a broad peak near 2 eV. Indeed, when $V = \omega - \delta$, for small but positive δ, the hybrid state $\lambda_0^- = \delta$ comes close in energy with the ground state, favoring the energy transfer cascade driven by thermal fluctuations. Figure 1(b) presents the polariton energy $\langle\hat{H}_S\rangle$ near $V = \omega = 1$ eV at 300, 100, and 10 K. We observe a reduction in the

height and spread of this peak as the bath temperature drops, with a clear suppression of this peak at 10 K. This finding confirms that the energy absorption close to $V = \omega$ originates on the thermal fluctuations and the harmonic nature of the phonon. The second peak, centered at $V = 2\omega$, results from the emergence of a hybrid state with energy $\lambda_0^- = -\omega$, and the fact that the driving field frequency is in resonance with transition $\varepsilon_1 \to \lambda_0^-$. This resonant peak can be fit to a Lorentzian distribution with a scale parameter linearly depending on V and centered at 2 eV (see Appendix C). The energy contour in Fig. 1(c), reveals how the total polariton energy in resonance varies for different values in the damping rates Γ_X and Γ_P, suggesting that $\langle \hat{H}_S \rangle$ is more sensitive to Γ_P than Γ_X. We also note that majority of the polariton energy is stored in the phonon modes. Figure 1(d) shows that the system reaches a periodic stationary state. The energy oscillation amplitude in this stationary state is very small, on the order of a few μeV, as expected for an overdamped system with $A^2/\text{eV} < \Gamma_X, \Gamma_P$. These oscillations are not detectable from Fig. 1(d), and we can regard the polariton energy as constant. Figure 1(e) shows the density matrix diagonal elements for several values on the coupling strengths V, and as a function of the energy. These probabilities can be fit to a biexponential function with two energy decay parameters: one dominating at low energies, and the second one dominating at higher energies. Such biexponential fitting function is consistent with the definitions of $\hat{H}$ and $\hat{H}_d$ and the form for the density matrix in Eq. (7). Notably, while the population probabilities are maximal in resonance, their decay parameters do not change significantly with V.

We investigate the polariton quantum thermodynamics under periodic driving in Fig. 2. First, we calculate the heat and work rates defined in Eqs. (10)–(12) in the long-time evolution regime in Fig. 2(a). We find negative and constant $\dot{Q}_X$ and $\dot{Q}_P$, indicating a net flux of heat energy from the polariton to the environment, while the work done on the system oscillates as the driving field. The total work per period $\overline{W} \equiv \int_0^\tau \dot{W}(t)dt$, presented in Fig. 2(b), serves as a measure of the thermodynamic efficiency of the process as a function of the coupling strength. Indeed, for a specific realization of the system, the intensity of the external field enters in the definition of the parameter A in our model, which is kept constant in our calculations. The thermodynamic efficiency, defined by the ratio between $\overline{W}$ and the intensity of the external field, is therefore maximal in resonance ($\omega' = \omega$ and $V = 2\omega$) as it is in these conditions that $\overline{W}$ is maximal. We note that during the cyclic process imposed by external modulation, the polariton remains in a stationary state far from equilibrium. As a result, the efficiency described here cannot be compared with the Carnot efficiency, and it is therefore the figure of merit for the performance of the external pumping. Figure 2(c) shows the von Neumann entropy rates defined in Eq. (15) at resonance, and Fig. 2(d) presents the inverse effective temperature introduced in Eq. (16) as a function of V. We observe that β_{eff}^{-1} achieves its maximum value at resonance, and it quickly decays away from this point. With this effective temperature, we numerically verify energy balance and the first law in the stationary state in Fig. 2(e). We note that while $\dot{U}_S(t)$ oscillates on time, the environment's internal energy also oscillates, canceling the variation of the universe's internal energy at all times. Finally, in Fig. 2(f) we show the total irreversible heat

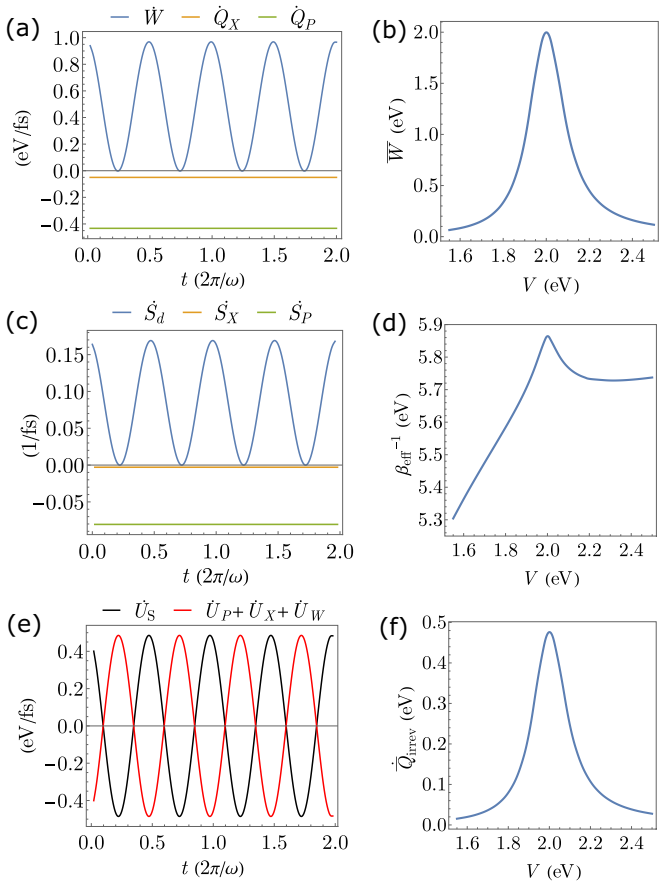

FIG. 2. Polariton quantum thermodynamics. (a) Work and heat rates as a function of time. (b) Total work $\overline{W}$ done in the polariton by the external source per period τ as a function of coupling strength V. (c) von Neumann entropy rates as a function of time. (d) Inverse effective temperature β_{eff}^{-1} as a function of V. (e) Polariton $\dot{U}_S$ and total reservoir $\dot{U}_P + \dot{U}_P + \dot{U}_P$ internal energy change rate as a function of time. (f) Total irreversible dissipated heat $\overline{Q}_{\text{irrev}}$ per period as a function of coupling strength V. These quantities are calculated after 8.271 ps of evolution. Parameters are as in Fig. 1.

dissipated per period $\overline{Q}_{\text{irrev}} \equiv \int_0^\tau \dot{Q}_{\text{irrev}}(t)dt$ as a function of V, and find that this quantity is also maximal in resonance.

V. CONCLUSION

We developed a robust and efficient model for periodically driven polaritons, weakly interacting with external reservoirs, in the strong-coupling regime. We utilized this formalism to reveal the polariton long-time evolution and thermodynamic performance upon external modulation. Significantly, our approach is not limited to the stationary case and can also be used to investigate the polariton transient dynamics and performance. Moreover, we believe that our formalism permits the study of the quantum thermodynamics of other analog systems.

ACKNOWLEDGMENTS

We thank the first reviewer for suggesting Ref. [31] and the references therein.

APPENDIX A: QUANTUM MASTER EQUATION

We solve the Liouville-von Neumann (LvN) equation for the full density matrix $\bar{\rho}(t)$, assuming that the surroundings remain in equilibrium during the driving, such that $\bar{\rho}(t) = \rho^{\mathrm{S}}(t) \otimes \rho^{\mathrm{B}}_{\mathrm{eq}}$ at all times. We write the LvN equation in the interaction picture

$$\frac{d\bar{\rho}_I}{dt} = -\frac{i}{\hbar}[\hat{\mathcal{V}}_I(t), \bar{\rho}_I(t)], \tag{A1}$$

with interaction Hamiltonian

$$\hat{\mathcal{V}}_I(t) = \hat{H}_I + \hat{H}_d(t) \tag{A2}$$

and

$$\bar{\rho}_I(t) = e^{+i\hat{H}_{\mathrm{S}}t/\hbar}\,\bar{\rho}(t)\,e^{-i\hat{H}_{\mathrm{S}}t/\hbar}, \tag{A3}$$

We solve Eq. (A1), f ollowing the Born-Markov approximations described in, e.g., Ref. [46]. First we integrate Eq. (A1)

$$\rho_I(t) - \rho_I(0) = -\frac{i}{\hbar}\int_0^t [\hat{\mathcal{V}}_I(t'), \bar{\rho}_I(t')]\,dt', \tag{A4}$$

and replace Eq. (A4) in Eq. (A1) to obtain

$$\frac{d\bar{\rho}_I}{dt} = -\frac{i}{\hbar}[\hat{\mathcal{V}}_I(t), \bar{\rho}_I(0)] - \frac{1}{\hbar^2}\int_0^t [\hat{\mathcal{V}}_I(t), [\hat{\mathcal{V}}_I(t'), \bar{\rho}_I(t')]]dt'. \tag{A5}$$

Next, we trace out the bath degrees of freedom assuming independent baths and that the polariton is initially in an equilibrium state $\rho^S(0) = \rho_{\mathrm{eq}}$:

$$\frac{d\rho^S_I}{dt} = -\frac{1}{\hbar^2}\int_0^t \mathrm{Tr}_B\{[\hat{\mathcal{V}}_I(t), [\hat{\mathcal{V}}_I(t'), \bar{\rho}_I(t')]]\}dt', \tag{A6}$$

and noting that

$$\frac{d\rho^S_I}{dt} = \frac{i}{\hbar}\big[\hat{H}_{\mathrm{S}}, \rho^S_I(t)\big] + e^{+i\hat{H}_{\mathrm{S}}t/\hbar}\,\frac{d\rho^S(t)}{dt}\,e^{-i\hat{H}_{\mathrm{S}}t/\hbar} \tag{A7}$$

We finally obtain up to second order in W_X, W_P, and A

$$\frac{d}{dt}\rho^{\mathrm{S}}(t) = -\frac{i}{\hbar}[\hat{H}_{\mathrm{S}}, \rho^{\mathrm{S}}(t)] - \frac{1}{\hbar^2}\int_0^t e^{-i\hat{H}_{\mathrm{S}}t/\hbar} \times \mathrm{Tr}_B\big\{\big[\hat{\mathcal{V}}_I(t), \big[\hat{\mathcal{V}}_I(t'), \rho^{\mathrm{S}}_I(t')\big]\big]\big\}e^{-i\hat{H}_{\mathrm{S}}t/\hbar}\,dt'. \tag{A8}$$

From the first term in the right hand side in Eq. (A8) we recover $\mathcal{D}$

$$\frac{\partial}{\partial t}\rho^{\alpha}_{\beta}(t) = -i(\lambda_\alpha - \lambda_\beta)\rho^{\alpha}_{\beta}(t). \tag{A9}$$

The second term incorporates the effect of the coupling of the polariton to the environment and the external driving, which are represented by the operators $\mathcal{L}_X$, $\mathcal{L}_P$, and $\mathcal{L}_d$ in the main text. Since the derivation of $\mathcal{L}_X$ and $\mathcal{L}_P$ follow a similar pattern, we illustrate this derivation in some detail for $\mathcal{L}_P$ and indicate how $\mathcal{L}_X$ results from simple substitutions.

First, we introduce the self-energies

$$\Sigma^{P,>}(t,t') = \sum_k \big|W^P_k\big|^2\langle\hat{b}_k(t)\hat{b}^\dagger_k(t')\rangle_B \tag{A10}$$

$$\Sigma^{P,<}(t,t') = \sum_k \big|W^P_k\big|^2\langle\hat{b}^\dagger_k(t)\hat{b}_k(t')\rangle_B \tag{A11}$$

and adopt a Markovian approximation to the dynamics in Eq. (A8) by replacing $\rho_I(t') \to \rho_I(t)$. After this, we invoke the Redfield-Markov approximation and change the integral domain from $(0,t)$ to $(-\infty,\infty)$, with a rescaling $1/2$ factor such that $\int_0^t \to \frac{1}{2}\int_{-\infty}^{\infty}$. The eight terms resulting from the explicit evaluation of the commutators in the second term in Eq. (A8) are

$$\begin{aligned}\mathcal{L}_{P\,\alpha_2\beta_2}^{\alpha_1\beta_1} &= \int_{-\infty}^{\infty}\tilde{\mathcal{L}}_{P\,\alpha_2\beta_2}^{\alpha_1\beta_1}(t,t')dt' \\ &= \Gamma_P\sum_\gamma \big(n(\gamma,\beta_1)\,\hat{a}^{\alpha_1}_{\gamma}\hat{a}^{\dagger\gamma}_{\alpha_2} \\ &\quad + (1+n(\gamma,\beta_1))\,\hat{a}^{\dagger\alpha_1}_{\gamma}\hat{a}^{\gamma}_{\alpha_2}\big)\delta^{\beta_1}_{\beta_2} \\ &\quad - \big(n(\alpha_1,\gamma)\,\hat{a}^{\dagger\alpha_1}_{\alpha_2}\hat{a}^{\beta_2}_{\beta_1} + (1+n(\alpha_1,\gamma))\,\hat{a}^{\alpha_1}_{\alpha_2}\hat{a}^{\dagger\beta_2}_{\beta_1}\big)\delta^{\beta_2}_{\gamma} \\ &\quad + \big(n(\gamma,\alpha_2)\,\hat{a}^{\beta_2}_{\gamma}\hat{a}^{\dagger\gamma}_{\beta_1} + (1+n(\gamma,\alpha_2))\,\hat{a}^{\dagger\beta_2}_{\gamma}\hat{a}^{\gamma}_{\beta_1}\big)\delta^{\alpha_2}_{\alpha_1} \\ &\quad - \big(n(\beta_1,\alpha_2)\,\hat{a}^{\dagger\alpha_1}_{\alpha_2}\hat{a}^{\gamma}_{\beta_1} + (1+n(\beta_1,\alpha_2))\,\hat{a}^{\alpha_1}_{\alpha_2}\hat{a}^{\dagger\gamma}_{\beta_1}\big)\delta^{\gamma}_{\beta_2}\end{aligned} \tag{A12}$$

with $\Gamma_P = 2\pi\sum_k |W^P_k|^2\delta(\omega_k - \omega)$. In this work we invoke the wideband approximation. This is justified under the assumption that Γ_P is small compared to the width of the spectral function. As indicated above, $\mathcal{L}_X$ follows from similar considerations and under the substitution $\hat{b}_k \to \hat{c}_k$, $\hat{a} \to \hat{d}^\dagger_1\hat{d}_2$, and $W_P \to W_X$.

For the driving field introduced in Eq. (5) we write

$$\hat{x} = \hat{d}^\dagger_1\hat{d}_2 = \sum_m |1,m\rangle\langle 2,m| \tag{A13}$$

and evaluate the double commutator in Eq. (A8) under the Markovian approximations described above. For this we note that ($\hbar = 1$)

$$\begin{aligned}&\int_{-\infty}^{\infty} dt'\cos(\omega t)\cos(\omega t')e^{-i\Delta\lambda(t'-t)} \\ &\quad = \pi\cos(\omega t)(e^{i\omega t}\delta(\Delta\lambda - \omega) + e^{-i\omega t}\delta(\Delta\lambda + \omega)),\end{aligned} \tag{A14}$$

and as a resu lt

$$\begin{aligned}\mathcal{L}_{d\,\alpha_2\beta_2}^{\alpha_1\beta_1}(t) &= -2|A|^2\cos(\omega' t) \\ &\quad\times\Bigg\{(g(\beta_1,\alpha_2,\omega',t) + g(\beta_2,\alpha_1,\omega',t)) \\ &\quad\times\big(\hat{x}^{\dagger\alpha_2}_{\alpha_1}\hat{x}^{\beta_1}_{\beta_2} + \hat{x}^{\alpha_2}_{\alpha_1}\hat{x}^{\dagger\beta_1}_{\beta_2}\big) \\ &\quad - \sum_\gamma\big(g(\beta_1,\gamma,\omega',t)\big(\hat{x}^{\dagger\gamma}_{\alpha_1}\hat{x}^{\alpha_2}_{\gamma} + \hat{x}^{\gamma}_{\alpha_1}\hat{x}^{\dagger\alpha_2}_{\gamma}\big)\delta^{\beta_1}_{\beta_2} \\ &\quad + g(\gamma,\alpha_1,\omega',t)\big(\hat{x}^{\dagger\gamma}_{\beta_2}\hat{x}^{\beta_1}_{\gamma} + \hat{x}^{\gamma}_{\beta_2}\hat{x}^{\dagger\beta_1}_{\gamma}\big)\delta^{\alpha_1}_{\alpha_2}\big)\Bigg\},\end{aligned} \tag{A15}$$

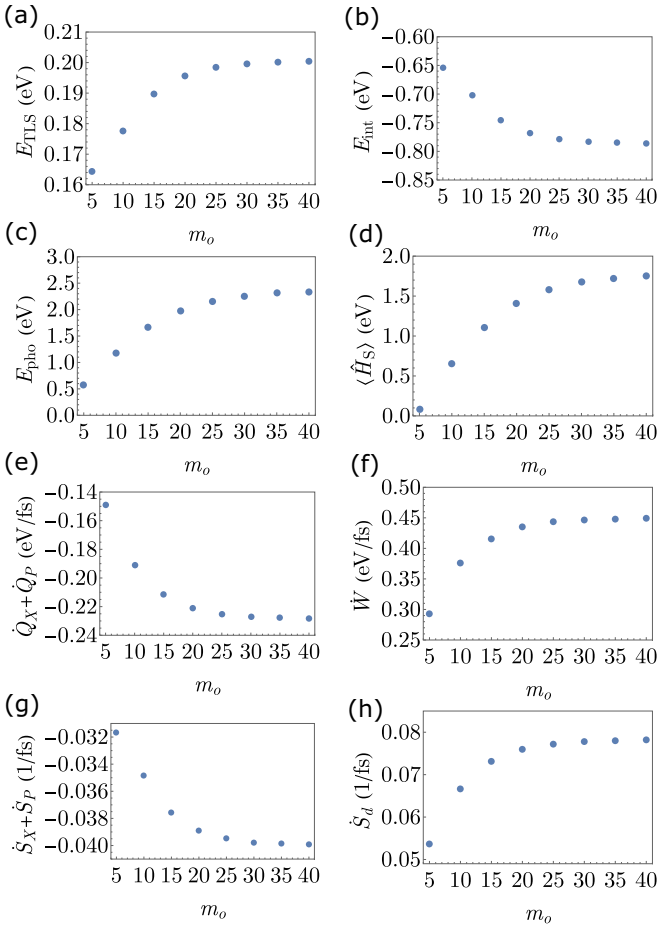

FIG. 3. Absolute energies, heat, work, and von Neumann entropy rates as a function of the upper bound in the number of phonon modes m_o, for the system in Figs. 1 and 2, for $V = 1.9\omega$, $\tau = 2000\tau = 8.271$ ps, $\Gamma_P = 0.16$ e V $= 4\Gamma_X$. Other parameters are as in Figs. 1 and 2.

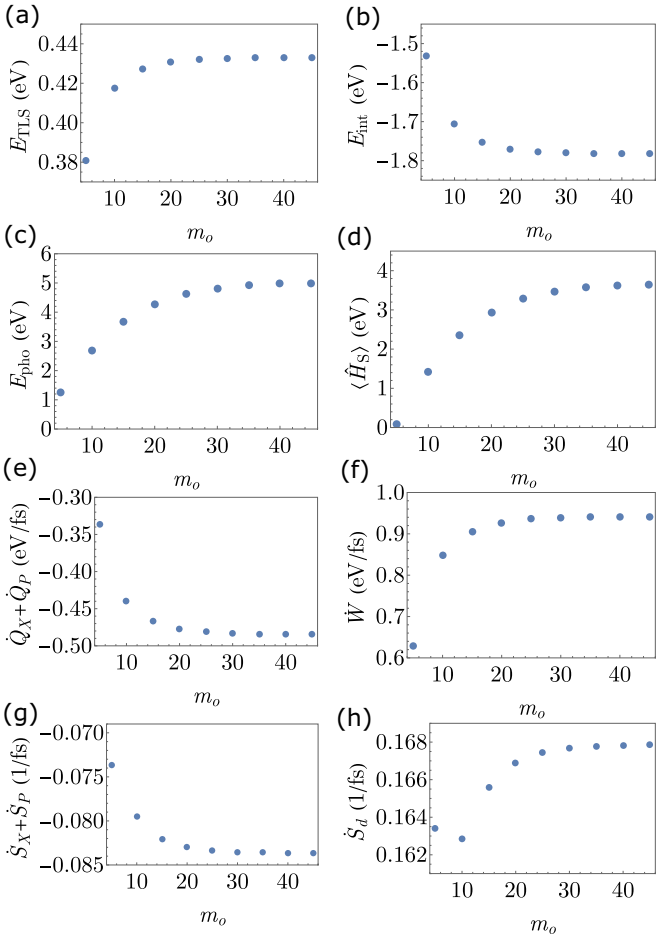

FIG. 4. Absolute energies, heat, work, and von Neumann entropy rates as a function of the upper bound in the number of phonon modes m_o, for the system in Figs. 1 and 2, for $V = 2\omega$, $\tau = 2000\tau = 8.271$ ps, $\Gamma_P = 0.16$ e V $= 4\Gamma_X$. Other parameters are as in Figs. 1 and 2.

where

$$g(\alpha, \beta, \omega, t) = e^{i\omega t}\delta(\lambda_\alpha - \lambda_\beta - \omega) + e^{-i\omega t}\delta(\lambda_\alpha - \lambda_\beta + \omega). \tag{A16}$$

From Eq. (A15), we obtain the transition matrices, $\mathcal{N}_\pm$, defined in Eq. (8)

$$\begin{aligned}\mathcal{N}_{\pm\,\alpha_2\beta_2}^{\alpha_1\beta_1} = \Big\{ &\big(\delta(\lambda_{\beta_1} - \lambda_{\alpha_2} \mp \omega') + \delta(\lambda_{\beta_2} - \lambda_{\alpha_1} \mp \omega')\big) \\ &\times \big(\hat{x}^{\dagger\alpha_2}_{\alpha_1}\hat{x}^{\beta_1}_{\beta_2} + \hat{x}^{\alpha_2}_{\alpha_1}\hat{x}^{\dagger\beta_1}_{\beta_2}\big) \\ &- \sum_\gamma \big(\delta(\lambda_{\beta_1} - \lambda_\gamma \mp \omega')\big(\hat{x}^{\dagger\gamma}_{\alpha_1}\hat{x}^{\alpha_2}_{\gamma} + \hat{x}^{\gamma}_{\alpha_1}\hat{x}^{\dagger\alpha_2}_{\gamma}\big)\delta^{\beta_1}_{\beta_2} \\ &+ \delta(\lambda_\gamma - \lambda_{\alpha_1} \mp \omega')\big(\hat{x}^{\dagger\gamma}_{\beta_2}\hat{x}^{\beta_1}_{\gamma} + \hat{x}^{\gamma}_{\beta_2}\hat{x}^{\dagger\beta_1}_{\gamma}\big)\delta^{\alpha_1}_{\alpha_2}\big)\Big\}. \end{aligned} \tag{A17}$$

In our calculations involving Eqs. (A16) and (A17), we approximate the Dirac's delta function by a Lorentzian function with broadening parameters equal to 1×10^{-4} eV.

APPENDIX B: NUMERICAL CONVERGENCE TESTS

In this section we provide evidence for the numerical convergence of the energy and thermodynamic rates reported in Figs. 1 and 2 when we carry out the summation over the phonon modes including only the first thirty modes ($m_o = 30$). In Figs. 3 and 4 we present the energies $E_{\rm TLS}$, $E_{\rm int}$, $E_{\rm pho}$, and $\langle \hat{H}_S \rangle$; the heat and work rates $\dot{Q}_X + \dot{Q}_P$ and $\dot{W}$; the von Neumann entropy rates $\dot{S}_X + \dot{S}_P$ and $\dot{S}_d$ correspondingly off-resonance ($V = 1.9\omega$) and in resonance($V = 2\omega$) for $t = 2000\tau = 8.271$ ps. We find that the energy rates converge to the numerical exact value for $m_o = 30$. We also note that $E_{\rm pho}$ and $\langle \hat{H}_S \rangle$ deviate about 3% from the limit value in resonance ($m_o = 45$). This deviation is not relevant for the thermodynamic analysis.

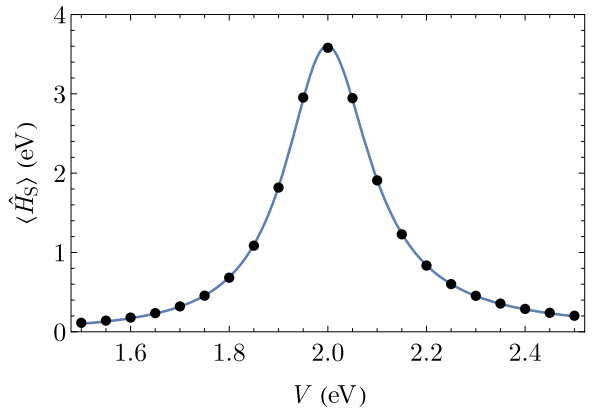

FIG. 5. Polariton energy near $V = 2\omega$, obtained from the density matrix (dots) and from the fitting function in Eq. (C1). Other parameters are as in Fig. 1(a).

APPENDIX C: LINESHAPE NEAR RESONANCE

In this section we show that we can fit the second peak in Fig. 1(a), centered at $V = 2\omega$, to a Lorentzian form with a broadening parameter that linearly depends on the exciton-phonon coupling strength. Explicitly, we write $\langle \hat{H}_S \rangle$ as function of V

$$\langle \hat{H}_S \rangle = 0.376 * \frac{(0.0696V - 0.0349)}{(V - 2.0)^2 + (0.0696V - 0.0349)^2} \quad \text{(C1)}$$

Figure 5 presents a comparison between the energies obtained as the expectation value of H_S and the ones obtained from the fitting function in Eq. (C1).

[1] T. E. Li, B. Cui, J. E. Subotnik, and A. Nitzan, Molecular polaritonics: Chemical dynamics under strong light–matter coupling, Annu. Rev. Phys. Chem. **73**, 43 (2021).

[2] A. D. Dunkelberger, B. S. Simpkins, I. Vurgaftman, and J. C. Owrutsky, Vibration-cavity polariton chemistry and dynamics, Annu. Rev. Phys. Chem. **73**, 429 (2022).

[3] N. T. Fofang, N. K. Grady, Z. Fan, A. O. Govorov, and N. J. Halas, Plexciton dynamics: exciton- plasmon coupling in a j-aggregate- au nanoshell complex provides a mechanism for nonlinearity, Nano Lett. **11**, 1556 (2011).

[4] M. Mondal, M. A. Ochoa, M. Sukharev, and A. Nitzan, Coupling, lifetimes, and strong coupling maps for single molecules at plasmonic interfaces, J. Chem. Phys. **156**, 154303 (2022).

[5] M. Mondal, A. Semenov, M. A. Ochoa, and A. Nitzan, Strong coupling in infrared plasmonic cavities, J. Phys. Chem. Lett. **13**, 9673 (2022).

[6] R. I. Kaitouni, O. ElDaif, A. Baas, M. Richard, T. Paraiso, P. Lugan, T. Guillet, F. Morier-Genoud, J.D. Ganiere, J.L. Staehli, V. Savona, and B. Deveaud, Engineering the spatial confinement of exciton polaritons in semiconductors, Phys. Rev. B **74**, 155311 (2006).

[7] H. Deng, H. Haug, and Y. Yamamoto, Exciton-polariton bose-einstein condensation, Rev. Mod. Phys. **82**, 1489 (2010).

[8] M. A. Ochoa, J. E. Maslar, and H. S. Bennett, Extracting electron densities in n-type gaas from raman spectra: Comparisons with hall measurements, J. Appl. Phys. **128**, 075703 (2020).

[9] W. Khan, P. P. Potts, S. Lehmann, C. Thelander, K. A. Dick, P. Samuelsson, and V. F. Maisi, Efficient and continuous microwave photoconversion in hybrid cavity-semiconductor nanowire double quantum dot diodes, Nat. Commun. **12**, 1 (2021).

[10] E. V. Denning, M. Wubs, N. Stenger, J. Mørk, and P. T. Kristensen, Cavity-induced exciton localization and polariton blockade in two-dimensional semiconductors coupled to an electromagnetic resonator, Phys. Rev. Res. **4**, L012020 (2022).

[11] B. Pigeau, S. Rohr, L. Mercier de Lépinay, A. Gloppe, V. Jacques, and O. Arcizet, Observation of a phononic mollow triplet in a multimode hybrid spin-nanomechanical system, Nat. Commun. **6**, 8603 (2015).

[12] P.-B. Li, Z.-L. Xiang, P. Rabl, and F. Nori, Hybrid Quantum Device with Nitrogen-Vacancy Centers in Diamond Coupled to Carbon Nanotubes, Phys. Rev. Lett. **117**, 015502 (2016).

[13] C. S. Muñoz, A. Lara, J. Puebla, and F. Nori, Hybrid Systems for the Generation of Nonclassical Mechanical States via Quadratic Interactions, Phys. Rev. Lett. **121**, 123604 (2018).

[14] G. Kurizki, P. Bertet, Y. Kubo, K. Mølmer, D. Petrosyan, P. Rabl, and J. Schmiedmayer, Quantum technologies with hybrid systems, Proc. Natl. Acad. Sci. **112**, 3866 (2015).

[15] J. P. Pekola, Towards quantum thermodynamics in electronic circuits, Nat. Phys. **11**, 118 (2015).

[16] M. Esposito, M. A. Ochoa, and M. Galperin, Quantum Thermodynamics: A Nonequilibrium Green's Function Approach, Phys. Rev. Lett. **114**, 080602 (2015).

[17] S. Vinjanampathy and J. Anders, Quantum thermodynamics, Contemp. Phys. **57**, 545 (2016).

[18] S. Deffner and S. Campbell, *Quantum Thermodynamics: An Introduction to the Thermodynamics of Quantum Information* (Morgan & Claypool Publishers, San Rafael, 2019).

[19] R. Kosloff, Quantum thermodynamics and open-systems modeling, J. Chem. Phys. **150**, 204105 (2019).

[20] P. Talkner, E. Lutz, and P. Hänggi, Fluctuation theorems: Work is not an observable, Phys. Rev. E **75**, 050102(R) (2007).

[21] M. Esposito, M. A. Ochoa, and M. Galperin, Nature of heat in strongly coupled open quantum systems, Phys. Rev. B **92**, 235440 (2015).

[22] R. S. Whitney, R. Sánchez, and J. Splettstoesser, Quantum thermodynamics of nanoscale thermoelectrics and electronic devices, in *Thermodynamics in the Quantum Regime* (Springer, Switzerland, 2018), pp. 175–206.

[23] A. A. S. Kalaee and A. Wacker, Positivity of entropy production for the three-level maser, Phys. Rev. A **103**, 012202 (2021).

[24] M. Esposito, M. A. Ochoa, and M. Galperin, Efficiency fluctuations in quantum thermoelectric devices, Phys. Rev. B **91**, 115417 (2015).

[25] M. F. Ludovico, J. S. Lim, M. Moskalets, L. Arrachea, and D. Sánchez, Dynamical energy transfer in ac-driven quantum systems, Phys. Rev. B **89**, 161306(R) (2014).
[26] A. Bruch, M. Thomas, S. V. Kusminskiy, F. Von Oppen, and A. Nitzan, Quantum thermodynamics of the driven resonant level model, Phys. Rev. B **93**, 115318 (2016).
[27] P. Haughian, M. Esposito, and T. L. Schmidt, Quantum thermodynamics of the resonant-level model with driven system-bath coupling, Phys. Rev. B **97**, 085435 (2018).
[28] M. A. Ochoa, N. Zimbovskaya, and A. Nitzan, Quantum thermodynamics for driven dissipative bosonic systems, Phys. Rev. B **97**, 085434 (2018).
[29] E. Aurell and R. Eichhorn, On the von neumann entropy of a bath linearly coupled to a driven quantum system, New J. Phys. **17**, 065007 (2015).
[30] S.-W. Li *et al.*, Production rate of the system-bath mutual information, Phys. Rev. E **96**, 012139 (2017).
[31] R. Alicki, The quantum open system as a model of the heat engine, J. Phys. A: Math. Gen. **12**, L103 (1979).
[32] R. Hotz and G. Schaller, Coarse-graining master equation for periodically driven systems, Phys. Rev. A **104**, 052219 (2021).
[33] Y. Tanimura, Numerically exact approach to open quantum dynamics: The hierarchical equations of motion (heom), J. Chem. Phys. **153**, 020901 (2020).
[34] A. Wacker, Nonresonant two-level transitions: Insights from quantum thermodynamics, Phys. Rev. A **105**, 012214 (2022).
[35] D. W. Hone, R. Ketzmerick, and W. Kohn, Statistical mechanics of floquet systems: The pervasive problem of near degeneracies, Phys. Rev. E **79**, 051129 (2009).
[36] S. Restrepo, J. Cerrillo, P. Strasberg, and G. Schaller, From quantum heat engines to laser cooling: Floquet theory beyond the born–markov approximation, New J. Phys. **20**, 053063 (2018).
[37] C. Deng, F. Shen, S. Ashhab, and A. Lupascu, Dynamics of a two-level system under strong driving: Quantum-gate optimization based on floquet theory, Phys. Rev. A **94**, 032323 (2016).
[38] M. A. Ochoa, Y. Selzer, U. Peskin, and M. Galperin, Pump–probe noise spectroscopy of molecular junctions, J. Phys. Chem. Lett. **6**, 470 (2015).
[39] C. Elouard, D. Herrera-Martí, M. Esposito, and A. Auffèves, Thermodynamics of optical bloch equations, New J. Phys. **22**, 103039 (2020).
[40] M. A. Ochoa, A. Bruch, and A. Nitzan, Energy distribution and local fluctuations in strongly coupled open quantum systems: The extended resonant level model, Phys. Rev. B **94**, 035420 (2016).
[41] M. Bamba and T. Ogawa, Dissipation and detection of polaritons in the ultrastrong-coupling regime, Phys. Rev. A **86**, 063831 (2012).
[42] L. Sieberer, S. D. Huber, E. Altman, and S. Diehl, Dynamical Critical Phenomena in Driven-Dissipative Systems, Phys. Rev. Lett. **110**, 195301 (2013).
[43] A. Drezet, Quantizing polaritons in inhomogeneous dissipative systems, Phys. Rev. A **95**, 023831 (2017).
[44] T. Pistorius, J. Kazemi, and H. Weimer, Quantum Many-Body Dynamics of Driven-Dissipative Rydberg Polaritons, Phys. Rev. Lett. **125**, 263604 (2020).
[45] A more general driving protocol will also include direct coupling to the phonon, e.g., in the following form

$$2A' \cos(\omega' t) \sum_{i\in\{1,2\}} \sum_{m} |i, m\rangle\langle m+1, i| + |i, m+1\rangle\langle m, i|,$$

with interaction strength A'. It is possible to account for the dynamic and thermodynamic contributions of such interaction within the present formalism as this results in an additional time-dependent operator similar to $\mathcal{L}_d$, entering linearly in Eq. (6).
[46] H.-P. Breuer, F. Petruccione *et al.*, *The Theory of Open Quantum Systems* (Oxford University Press on Demand, Oxford 2002).
[47] E. Davidsson and M. Kowalewski, Simulating photodissociation reactions in bad cavities with the lindblad equation, J. Chem. Phys. **153**, 234304 (2020).
[48] M. Du, J. A. Campos-Gonzalez-Angulo, and J. Yuen-Zhou, Nonequilibrium effects of cavity leakage and vibrational dissipation in thermally activated polariton chemistry, J. Chem. Phys. **154**, 084108 (2021).
[49] H. Spohn, Entropy production for quantum dynamical semigroups, J. Math. Phys. **19**, 1227 (1978).